




## Isolated spectrally discrete bound states in the continuum in an open system

Samyabrata Mukherjee <sup>1</sup>, Jordi Gomis-Bresco<sup>1</sup>, David Artigas <sup>1,2</sup> and Lluís Torner<sup>1,2,\*</sup>

<sup>1</sup>*ICFO-Institut de Ciències Fotòniques, The Barcelona Institute of Science and Technology, 08860 Castelldefels (Barcelona), Spain*

<sup>2</sup>*Department of Signal Theory and Communications, Universitat Politècnica de Catalunya, 08034 Barcelona, Spain*

 (Received 27 April 2023; revised 18 July 2023; accepted 25 October 2023; published 13 November 2023)

Bound states in the continuum (BICs) exist in a variety of physical systems where they appear as lossless propagating states surrounded by radiating modes. In the case of open systems, they coexist with continuous families of guided states, which may be modes or other BICs, located in different regions of the frequency-momentum parameter space. Here we report anisotropic waveguiding structures where guided modes and BICs protected by symmetry are not possible whatsoever, though an isolated, single interference BIC emerges as a lossless, solitary needle from a sea of radiating states. The needle BIC is the unique possible bound state, which originates from the interplay of the two different radiation channels present in the structure, and remarkably, it exists at a single frequency and a precise propagation direction as a spectrally discrete bound state for any practical range of frequencies.

DOI: [10.1103/PhysRevA.108.053506](https://doi.org/10.1103/PhysRevA.108.053506)

### I. INTRODUCTION

Bound states in the continuum (BICs) are modes that propagate without losses even though their existence domain overlaps with the part of the parameter space that corresponds to radiating waves. They were predicted in the context of quantum mechanics by von Neumann and Wigner [1], and this research was later extended by Stillinger and Herrick [2]. Subsequently, Friedrich and Wintgen described BICs as a general wave phenomenon [3], and since then they have been observed in many physical settings, including acoustic systems [4] and photonic systems, where they have inspired a wealth of new phenomena and important applications [5–8].

Pioneering works in photonics found BICs in dielectric gratings [9], photonic crystal waveguides [10], waveguide arrays [11,12], and photonic crystal slabs [13]. These studies spurred research into many systems, such as hybrid plasmonic-photonic systems [14,15], zero-index materials [16,17], diffraction gratings [18], slab waveguides with grooves [19] and ridge terminations [20], all-dielectric [21,22], plasmonic [23], and intrinsically chiral [24] metasurfaces, and several periodic systems [25–29], among others. Apart from periodic structures, photonic BICs also occur in anisotropic structures including waveguides [30,31], in structures containing anisotropic defect layers [32–34], and at interfaces as Dyakonov BICs [35]. In addition to being of fundamental interest, the existence of photonic BICs has been harnessed to realize applications in lasers [36,37], biosensing [38], multiplexed communication channels [39], directional radiation [40,41], broadband light capture [42], high-quality-factor (high- $Q$ ) resonators [43,44], and nonlinear optics [45,46], to cite a few examples.

The aforementioned settings exhibit BICs that appear in the dispersion space as isolated dots or as lines inserted within the leaky-mode branches forming the continuum. When considering the whole parameter space, such BICs coexist with numerous other BICs—either protected by symmetry or generated by interference—and, importantly, with bands of guided modes which occupy different parts of the parameter space. For example, symmetric photonic crystal slabs can support various accidental BICs, which coexist both with BICs protected by symmetry at the  $\Gamma$  point and branches of standard guided Bloch modes that exist below the light cone [13]. Practical applications of BICs thus use excitation methods [47,48] that avoid multiple resonances. Here we report a system allowing for the existence of an isolated, discrete, interference BIC that is the sole bound state possible in the whole available parameter space. This phenomenon occurs in antiguiding anisotropic structures where no guided modes are allowed and where such a state appears as an isolated, needlelike spectrally discrete BIC in the frequency-momentum dispersion diagram.

Anisotropy-induced BICs appear in planar structures composed of a substrate, film (or core), and cladding, where at least the substrate is anisotropic [30]. When all optical axes (OAs) are contained in the plane of the structure and parallel, the structure is anisotropy symmetric, and BICs appear as continuous lines that span over broad regions of the dispersion diagram. This is the case in structures where all three layers consist of uniaxial materials and the cladding and the substrate radiation channels become equivalent, e.g., due to geometric or mirror symmetry [49]. When at least one OA is taken out of the plane, the polar anisotropy symmetry is broken, showing groups of discrete BICs lying close to each other in the frequency-momentum space [50]. Here we address BICs in structures where the refractive indices of the anisotropic film are lower than the ordinary refractive index of the substrate and cladding, resulting in a so-called antiguiding structure, i.e., no standard guided modes are supported. The conditions

\*lluís.torner@icfo.eu

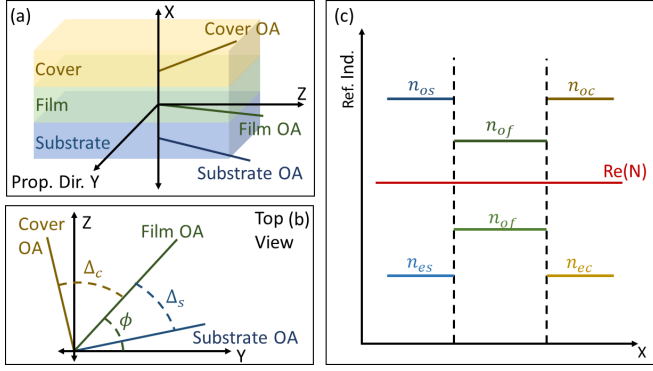


FIG. 1. (a) Layout of the system. The yellow, green, and blue lines show the optic axes (OAs) for the cover, film, and substrate, respectively. The OAs are parallel to the interface ( $y$ - $z$  plane). The coordinate system is aligned along the wave propagation direction  $y$ , and  $x$  is perpendicular to the interface. (b) The OA arrangement shown from the top. The angle  $\phi$  between the propagation direction ( $y$ ) and the film OA is shown along with the offsets  $\Delta_c$  ( $\Delta_s$ ) between the film OA and the cover (substrate) OA. (c) Schematic of the refractive indices showing three uniaxial materials with negative birefringence. The red line indicates the value of  $\text{Re}(N)$  for the modes that we study. Prop. Dir., propagation direction; Ref. Ind., refractive index.

for radiation suppression and BIC formation are then studied, showing that the inclusion of a second distinct radiation channel induces a transition where BIC lines in the dispersion diagram collapse into a single BIC point. Such a state turns out to be the only bound state existing for any practical range of frequencies and propagation directions and therefore results in a spectrally discrete needle BIC.

## II. THEORETICAL FORMULATION

In this section we introduce the formulation for the analysis of structures composed of film media sandwiched between a substrate and a cover or cladding, where all three media are lossless, dielectric uniaxial negative birefringent materials, with all OAs parallel to the interface plane ( $y$ - $z$ ) and having identical materials in the cladding and substrate [Fig. 1(a)]. To put our findings into perspective, we review the concept of guided and leaky modes and then focus on the simplest structure supporting needlelike BICs, which is a planar *antiguiding* structure. Finally, the condition for BIC existence is presented.

### A. The anisotropic structure

Figures 1(a) and 1(b) show the structure used in this paper. Since all three media are uniaxial with negative birefringence and the cladding and substrate comprise identical materials, their refractive indices fulfill  $n_{oc} = n_{os} > n_{ec} = n_{es}$ , and in the film  $n_{of} > n_{ef}$ , where the subscripts  $o$  and  $e$  refer to the ordinary and extraordinary indices, and  $c$ ,  $f$ , and  $s$  denote the cladding or cover, the film, and the substrate, respectively. The coordinate axes are centered at the substrate-film interface, where  $x$  is normal to the interface plane,  $y$  is the propagation direction, and  $\phi$  gives the angle between the film OA and the direction of propagation. Then, the permittivity tensor for a

given layer when the optic axis points in the  $y$  direction is given by

$$\hat{\epsilon} = \text{diag}(n_o^2, n_e^2, n_o^2). \quad (1)$$

The optic axis orientation in each layer transforms  $\hat{\epsilon}$  using the appropriate rotation matrix  $R_x(\phi)$ .

To have independent control over the cladding and substrate radiation channels, their OAs are free to rotate independently in the interface plane.  $\Delta_c = \phi_c - \phi$  ( $\Delta_s = \phi_s - \phi$ ) gives the offset between the film OA and the cladding (substrate) OAs. An equivalent formulation would involve fixing the OA orientations and rotating the direction of propagation of light in the  $y$ - $z$  plane. In this case,  $\phi$  corresponds to the propagation direction, with  $\phi = \arctan(k_z/k_y)$  [50].

### B. Transfer matrix formalism

Solutions of Maxwell's equations in uniaxial materials are combinations of four basis waves: two with ordinary polarization and two with extraordinary polarization. Eigenmodes supported by slab waveguides comprising birefringent materials, however, are hybrid, made up of a combination of basis waves with both ordinary and extraordinary polarization in each layer [51], and are calculated in this paper using the formulation in Ref. [50]. First, we define the ordinary and extraordinary basis waves in each layer and construct the eigenvalue problem as outlined in Ref. [51], resulting in the eigenvectors

$$\vec{F}_o = \begin{bmatrix} \kappa_o \sin(\phi) \\ n_o^2 \sin(\phi) \\ -\kappa_o \cos(\phi) \\ \kappa_o^2 \cos(\phi) \end{bmatrix}, \quad \vec{F}_e = \begin{bmatrix} \kappa_o^2 \cos(\phi) \\ \epsilon_o \kappa_e \cos(\phi) \\ \epsilon_o \sin(\phi) \\ -\epsilon_o \kappa_e \sin(\phi) \end{bmatrix}, \quad (2)$$

where the rows of  $\vec{F}_e$  and  $\vec{F}_o$  correspond to the tangential field components  $E_y$ ,  $z_0 H_z$ ,  $E_z$ , and  $z_0 H_y$ , respectively, and  $z_0$  is the vacuum impedance. We write the  $4 \times 4$  field matrix  $\hat{F}$  using Berreman's transfer matrix formalism [52], as

$$\hat{F} = [\vec{F}_o^+ \vec{F}_o^- \vec{F}_e^+ \vec{F}_e^-], \quad (3)$$

where the superscript  $+$  ( $-$ ) refers to basis waves propagating forward (backward) along  $x$ . The total field is calculated as  $\vec{m} = \hat{F} \vec{a}$ , where  $\vec{a}$  is a  $4 \times 1$ -column vector containing the amplitudes of the respective basis waves. The field can be transformed within two points in the same layer separated by a distance  $d$  using the phase matrix

$$\hat{A}_D = \text{diag}(e^{-ik_0 \kappa_o^+ D}, e^{-ik_0 \kappa_o^- D}, e^{-ik_0 \kappa_e^+ D}, e^{-ik_0 \kappa_e^- D}), \quad (4)$$

where  $\kappa_o$  and  $\kappa_e$  are the normalized propagation constants in the  $x$  direction for the ordinary and extraordinary basis waves. These are the eigenvalues of our problem, which can be related to the optical axis orientation in each layer,  $\phi$ , and the mode effective index  $N = k_y/k_0$  (normalized propagation

constant in the  $y$  direction) as

$$\begin{aligned}\kappa_o &= \pm \sqrt{n_o^2 - N^2}, \\ \kappa_e &= \pm \sqrt{n_e^2 - N^2 \left[ \sin^2(\phi) + \left( \frac{n_e^2}{n_o^2} \right) \cos^2(\phi) \right]}.\end{aligned}\quad (5)$$

Thus, using Eqs. (3) and (4), a  $4 \times 4$  characteristic matrix  $\hat{M}$  for a film of thickness  $D$  can be written as

$$\hat{M} = \hat{F}_f^{-1} \hat{A}_D \hat{F}_f, \quad (6)$$

where the subscript  $f$  refers to the film [51].

The cladding and the substrate are semi-infinite. Therefore only two (one ordinary and one extraordinary) out of the four basis waves must be selected for these layers. After selecting the appropriate basis waves in the cladding and the substrate, the fields at the two interfaces at  $x = 0$  and  $x = D$  are related using the characteristic matrix  $\hat{M}$  as

$$a_o^s \cdot \vec{F}_o^s + a_e^s \cdot \vec{F}_e^s = a_o^c \cdot \hat{M} \vec{F}_o^c + a_e^c \cdot \hat{M} \vec{F}_e^c, \quad (7)$$

where the superscript  $c$  ( $s$ ) denotes the cladding (substrate) and  $a_j^i$  is the complex amplitude of the corresponding basis wave. Rewriting Eq. (7), we obtain a homogeneous system of linear equations that can be written in matrix form as

$$\hat{W} \vec{a} = \begin{bmatrix} -\hat{M} \vec{F}_o^c & -\hat{M} \vec{F}_e^c & \vec{F}_o^s & \vec{F}_e^s \end{bmatrix} \vec{a} = 0. \quad (8)$$

The condition for the existence of nontrivial solutions of this homogeneous system of linear equations,  $|\hat{W}| = 0$ , gives us the dispersion equation which must be solved numerically to obtain the values of the effective mode index  $N$  for the hybrid eigenmodes supported by the structure.

### C. Guided and leaky modes

Guiding slab waveguides typically have films with higher refractive indices than the cladding and substrate and thus have  $N > [n_{oc}, n_{os}, n_{ec}, n_{es}]$ , with  $N$  being real. The value of  $\kappa_o$  and  $\kappa_e$  in the substrate and cover can be calculated using Eqs. (5). Guided modes have imaginary  $\kappa_o$  and  $\kappa_e$  and must decay in the substrate and cover as  $x \rightarrow \pm\infty$ , which is ensured by choosing the proper sign in Eqs. (5).

However, if  $N$  has a value smaller than any of the refractive indices for the cladding or the substrate ( $n_{os}, n_{oc}, n_{es}, n_{ec}$ ), then the corresponding value of  $\kappa_o$  or  $\kappa_e$  becomes real, and there is radiation leaking from the film to the substrate or the cover. This means that a radiation channel is opened in the cladding and/or the substrate, specifically, the ordinary or the extraordinary wave that corresponds to a refractive index larger than  $N$ , and for this value of  $N$ , guided modes are not supported, resulting instead in a continuum of radiating modes. This situation can be conveniently analyzed by using a formalism based on hybrid leaky modes made up of waves with both ordinary and extraordinary polarization [53–55]. These leaky modes are improper solutions of the dispersion equation that do not vanish as  $x \rightarrow \pm\infty$  [56], but provide a good approximation of the field near the waveguide and are characterized by a complex mode index  $N$ , where  $\text{Im}\{N\}$  approximates the radiation loss [56]. They are obtained as a solution of the dispersion equation by selecting the basis waves that grow exponentially upon moving away from the

interface for the polarization that corresponds to the radiation channel. For the other polarizations, evanescent waves that vanish as  $x \rightarrow \pm\infty$  are selected.

Antiguiging structures for any propagation direction  $\phi$  are ensured when the refractive indices fulfill  $n_{oc} = n_{os} > n_{ec} = n_{es}$ , and in the film,  $n_{os} > n_{of} > n_{ef} > n_{es}$  [Fig. 1(c)]. Here, the cladding and substrate ordinary refractive indices, which are independent of the OA orientation, are the highest ones in the structure. This has two important implications. First, light in the film would not remain confined and would couple to the continuum of ordinary waves in the cover and the substrate [30]. Therefore the structure cannot support any conventional guided mode, and only leaky modes are possible. Second, leaky modes in the structure will fulfill  $n_{ec} = n_{es} < \text{Re}\{N\} < n_{os} = n_{oc}$  [Fig. 1(c)]. Therefore the radiation channels in the cladding and substrate are the ordinary wave, which couple to the radiation continuum, while the extraordinary wave is evanescent.

Note that in addition to guided and leaky modes confined in the film, structures involving positive uniaxial materials can, under specific conditions, also support Dyakonov surface waves that remain confined at interfaces and decay exponentially away from the interface [57]. The existence of BICs in the context of Dyakonov surface waves has been recently studied [35], revealing that the interfaces between uniaxial positive and uniaxial negative materials can support guided and leaky Dyakonov surface waves, and that the leaky Dyakonov wave can become a surface BIC. However, the structures considered here are composed entirely of negative uniaxial materials, and that precludes the existence of Dyakonov surface waves. This is further confirmed by the electric field profiles of the leaky mode and the BIC [plotted in Figs. 3(b) and 3(c)], which show that light is confined within the film rather than at the interfaces.

### D. Conditions for BIC existence

For an interference (INT) BIC to exist, the amplitudes of the radiation channels, which in our case correspond to the ordinary polarization, must vanish via destructive interference, resulting in the conditions for radiation suppression. To obtain this condition, we set  $a_o^c = 0$  in Eq. (7) resulting in the condition for radiation suppression (by destructive interference) for the cladding,

$$a_o^s \cdot \vec{F}_o^s + a_e^s \cdot \vec{F}_e^s - a_e^c \cdot \hat{M} \vec{F}_e^c = 0, \quad (9)$$

and then set  $a_o^s = 0$  in Eq. (7) to obtain the conditions for radiation suppression for the substrate,

$$a_e^s \cdot \vec{F}_e^s - a_o^c \cdot \hat{M} \vec{F}_o^c - a_e^c \cdot \hat{M} \vec{F}_e^c = 0. \quad (10)$$

The condition for INT BIC existence in this structure with two radiation channels is set by requiring that the solutions coincide for Eqs. (7), (9), and (10) simultaneously. This approach, where two separate conditions for radiation suppression are defined for the two radiation channels, is not strictly necessary to study BICs and could be substituted by a single equation  $a_e^s \cdot \vec{F}_e^s = a_e^c \cdot \hat{M} \vec{F}_e^c$ , obtained by simultaneously setting  $a_o^c = 0$  and  $a_o^s = 0$  in Eq. (7). However, the use of two equations is more versatile, and this approach can also be used to

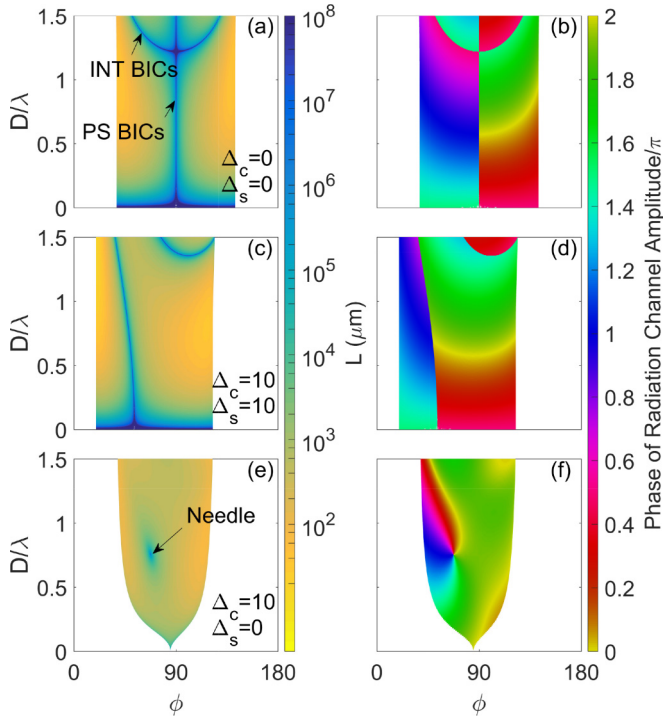


FIG. 2. BICs embedded on leaky modes and corresponding phase maps. (a), (c), and (e) Propagation length  $L = (k_0 \text{Im}\{N\})^{-1}$ , defined as the length at which the field amplitude decays to  $1/e$  of the initial value for the fundamental leaky mode, in terms of the film optical axis orientation (in degrees). (b), (d), and (f) The corresponding phase (in units of  $\pi$  radians) of the cladding radiation channel (ordinary) amplitude, measured with respect to the confined (extraordinary) wave. The OA orientations are as follows: (a) and (b)  $\Delta_c = \Delta_s = 0^\circ$ , (c) and (d)  $\Delta_c = \Delta_s = 10^\circ$ , and (e) and (f)  $\Delta_c = 10^\circ$ ,  $\Delta_s = 0^\circ$ . The transition from colored to white regions corresponds to the leaky-mode cutoff.

study phenomena such as unidirectional guided resonances in related geometries [49].

Mathematically, each condition for radiation suppression, given by Eqs. (9) and (10), comprises a system of four homogeneous linear equations, where each equation corresponds to one of the field components tangential to the interface encoded in vectors  $\vec{F}_i^j$  and provides the coefficients  $a_i^j$  for which interference suppresses the tangential component of the radiation channel. Written in matrix form, these overdetermined systems of four linear equations and three unknowns  $a_i^j$  have the form  $\hat{R}\vec{a} = 0$ , where  $\hat{R}$  is a  $4 \times 3$  matrix and  $\vec{a}$  is a  $3 \times 1$  column vector. Nontrivial solutions of this system require that the determinants of all four possible  $3 \times 3$  submatrices of  $\hat{R}$  equal zero, resulting in four different auxiliary equations for each condition for radiation suppression. Each auxiliary equation is a possible mathematical solution that suppresses the radiation channel when one of the tangential field components is ignored, specifically the component corresponding to the row left out when selecting the  $3 \times 3$  submatrix of  $\hat{R}$ . To ensure that the radiation channel is suppressed when all four tangential field components are taken into account, we must account for all the possible combinations of the tangential field components, and thus the solutions for the four auxiliary

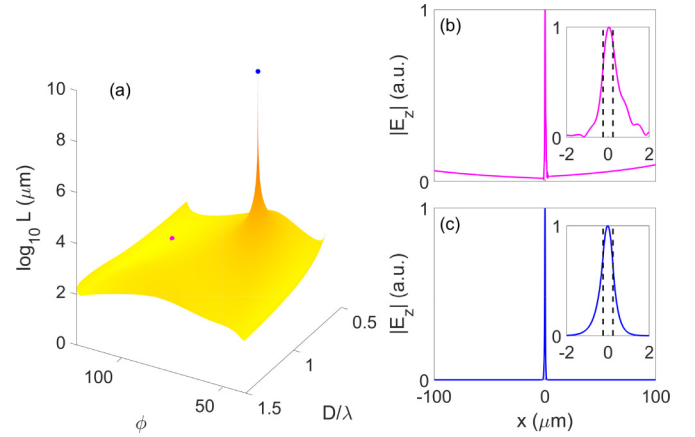


FIG. 3. (a) Propagation distance  $L$  in three dimensions, as a function of  $\phi$  and two octaves in  $D/\lambda$ . The needlelike isolated BIC is a lossless point surrounded by the radiating leaky mode within which it is embedded. The magenta and blue markers show the points for which the electric field profile ( $|E_z|$ ) is plotted in (b) for a leaky mode at  $D/\lambda = 0.758$  and  $\phi = 110^\circ$  and in (c) for the lossless needle BIC at the same value of  $D/\lambda$  but  $\phi = 67.6^\circ$ . The insets in (b) and (c) show the electric field profile near the waveguide. We consider an incident wavelength of  $\lambda = 0.632 \mu\text{m}$  for the field profile calculations. The dashed black lines indicate the waveguide interfaces.

equations must coincide. Accordingly, each auxiliary equation must be solved to obtain  $N_{\text{aux}}^{i,j}$ , where the index  $i$  runs over the four auxiliary equations and  $j = c, s$  refers to Eqs. (9) (cladding) and (10) (substrate), respectively. The solution for radiation suppression in the cladding is then at the point where the four different  $N_{\text{aux}}^{i,c}$  coincide in the parameter space. Similarly, the point of coincidence of the four different  $N_{\text{aux}}^{i,s}$  gives the point in the parameter space where radiation is suppressed in the substrate.

However, the coincidence of the solutions  $N_{\text{aux}}^{i,c}$  and  $N_{\text{aux}}^{i,s}$  does not necessarily imply that they are physical solutions since the field components must also satisfy Maxwell's equations and the associated boundary conditions, which are enforced by Eq. (7). Thus the intersection of the set of solutions of the auxiliary equations,  $N_{\text{aux}}^{i,j}$ , with the solution of the dispersion equation,  $N$ , obtained by solving Eq. (7) must be considered. For that, we define a metric to measure the distance of  $N_{\text{aux}}^{i,j}$  from the solution of the dispersion equation ( $N$ )

$$Q_j = \sqrt{\sum_{i=1}^4 |N - N_{\text{aux}}^{i,j}|^2}, \quad (11)$$

where the subscript in  $Q_j$ , with  $j = c, s$ , indicates the condition for radiation suppression corresponding to the cladding or the substrate, respectively. Then, the BIC exists at the point where  $Q_c$  and  $Q_s$  are simultaneously zero. Similarly, unidirectional guided resonances [49] exist when either  $Q_c = 0$  or  $Q_s = 0$ .

### III. RESULTS

We assume that our birefringent media are lossless dielectrics with real refractive indices and semi-infinite cladding and substrate. A typical signature of BIC existence is the presence of Fano resonances in the sample reflection or transmission spectra [58]. However, as commented before, guided modes do not propagate in the structure, and only hybrid leaky modes are supported. Therefore, in our setup, the signature of a BIC is an infinite propagation length. We thus plot the leaky-mode propagation length,  $L = (k_0 \text{Im}\{N\})^{-1}$ , which measures the  $1/e$  decay of the leaky modes, and the BICs occur when  $L$  diverges due to suppression of the radiation channels. In addition, the condition for BIC existence given by Eq. (11) unequivocally proves BIC existence. Finite structures, imperfect interfaces, material losses, or other perturbations would result in the BICs turning into quasi-BICs, which are leaky modes with low, but nonzero loss [59]. Furthermore, it is known that perfectly lossless BICs cannot occur in finite systems unless the permittivity or permeability vanishes or diverges [5]. However, since realistic samples would have dimensions that are  $10^3$  or  $10^4$  times the operating wavelength, in the calculations one can readily consider that the slabs of lossless dielectrics are infinite along the  $y$  and  $z$  directions and that the substrate and the cover extend infinitely in the  $-x$  and  $+x$  directions.

Without loss of generality, the antiguiding structure is made up of three negative uniaxial materials with cladding and substrate refractive indices  $n_{ec} = n_{es} = 1.3$  and  $n_{oc} = n_{os} = 1.7$  and film refractive indices  $n_{ef} = 1.4$  and  $n_{of} = 1.6$  so that the structure is symmetric in terms of refractive indices. All angles between optic axes ( $\phi$ ,  $\Delta$ ) in this paper are expressed in degrees.

#### A. Dispersion equation

When the structure has full anisotropy symmetry [50], i.e., the optic axes of the cladding, film, and substrate are aligned ( $\Delta_c = \Delta_s = 0^\circ$ ) and are parallel to the interface plane ( $\theta_c = \theta_f = \theta_s = 90^\circ$ ), the cladding and substrate radiation channels are equivalent, and the leaky mode supports families of both polarization-separable (PS) and interference (INT) BICs, which appear as lossless lines within the leaky-mode sheet in the  $\phi - D/\lambda$  space. This is shown in Fig. 2(a), which shows the propagation distance  $L$  for the fundamental branch of leaky modes. PS BICs are analogous to symmetry-protected BICs in other photonic structures [5,11] and exist at  $\phi = 90^\circ$ , where transverse electric (TE) and transverse magnetic (TM) modes are separable. Then PS BICs correspond to the TE modes supported by the guiding profile created by the extraordinary indices shown in Fig. 1(b). INT BICs are hybrid, full-vector modes that arise from destructive interference simultaneously in both radiation channels. As the anisotropy symmetry is maintained and the cladding and substrate radiation channels are equivalent, the fundamental leaky mode supports a curved line of existence of INT BICs [Fig. 2(a)]. Since BICs are zeros of radiation, the phase of the radiation channel amplitude at a BIC is undefined, and BIC existence loci result in a jump of  $\pm\pi$  in the phase of the radiation channel amplitude [50], as shown in Fig. 2(b) for the cladding

(the jump in phase of the substrate radiation channel at the loci of BIC lines is opposite in sign to that at the cladding).

Breaking the azimuthal anisotropy symmetry, but keeping identical OA orientations in the cladding and substrate ( $\Delta_c = \Delta_s \neq 0^\circ$ ), maintains the geometric mirror symmetry about  $x = D/2$  in the structure and the equivalence between the cladding and substrate radiation channels. Therefore the structure still supports lines of existence of BICs. However, all the lines are deformed and correspond to INT BICs only, as shown in Figs. 2(c) and 2(d) for  $\Delta_c = \Delta_s = 10^\circ$ . Thus this is weak anisotropy-symmetry breaking [50].

While BICs appear at isolated points in the parameter space in most photonic structures, where they coexist with other bound or guided modes, it has been known for some time that anisotropic structures can support lines of BICs embedded on leaky modes in certain geometries [30,50]. Note, however, that lines of BIC solutions have also been reported in the parameter space of photonic crystal slabs where the environment is engineered to also be a photonic crystal [28]. Besides, while the symmetry-protected BIC at the  $\Gamma$  point in photonic crystal slabs exists as long as mirror symmetry is maintained [29], the PS BIC in our structure disappears when anisotropy symmetry is broken, even if mirror symmetry is maintained.

Different OA orientations in the cladding and the substrate mean that, in addition to the anisotropy symmetry, the geometric mirror symmetry in the structure is also broken and the radiation channels are no longer equivalent. This situation is shown in Fig. 2(e) for the fundamental leaky mode, where the OA in the substrate is aligned with the OA in the film ( $\Delta_s = 0^\circ$ ) but the cladding OA has an offset  $\Delta_c = 10^\circ$ . As a result, a topological transition occurs in the leaky-mode map, and the BIC lines of existence shown in Figs. 2(a) and 2(c) collapse to an isolated BIC point [Fig. 2(e)]. The isolated BIC corresponds to a zero in both radiation channels and results in a phase singularity in the radiation channel amplitude characterized by a screw phase dislocation [44,50,60–62], as shown in Fig. 2(f). The BIC winding number is assigned according to the sense of the screw phase dislocation and has opposite sign in the cladding and substrate,  $-1$  (anticlockwise phase increase of  $2\pi$ ) and  $+1$  (clockwise increase), respectively [50,61]. Since anisotropy symmetry is broken, this structure cannot support PS BICs, and the BIC in Figs. 2(e) and 2(f) is an INT BIC with hybrid polarization. This BIC point, isolated in both wavelength and direction, is the only bound mode supported by the structure with these OA orientations (for these values of  $\phi$ ,  $\Delta_c$ , and  $\Delta_s$ ) over a broad range of frequencies  $D/\lambda$ . Specifically, the isolated BIC shown in Figs. 2(e) and 2(f) occurs at  $D/\lambda = 0.758$ , while the next BIC on the fundamental (zero order) leaky mode occurs at  $D/\lambda = 2.162$  (not shown), almost two octaves beyond. In the case of the first-order leaky mode, the first BIC appears even further beyond this, at  $D/\lambda = 2.682$ . Therefore the isolated BIC shown in Fig. 2(e) is the only bound mode supported by the structure for any practical operation range of wavelengths. Figure 3(a) shows how the propagation length  $L$  diverges, demonstrating the resemblance of the BIC to an isolated, lossless needle in an environment of radiating leaky modes. Figure 3(b) shows the profile of a tangential electric field component ( $|E_z|$ ) as a function of  $x$  for a point on the leaky mode shown in magenta in Fig. 3(a). The leakage from the core is shown in the

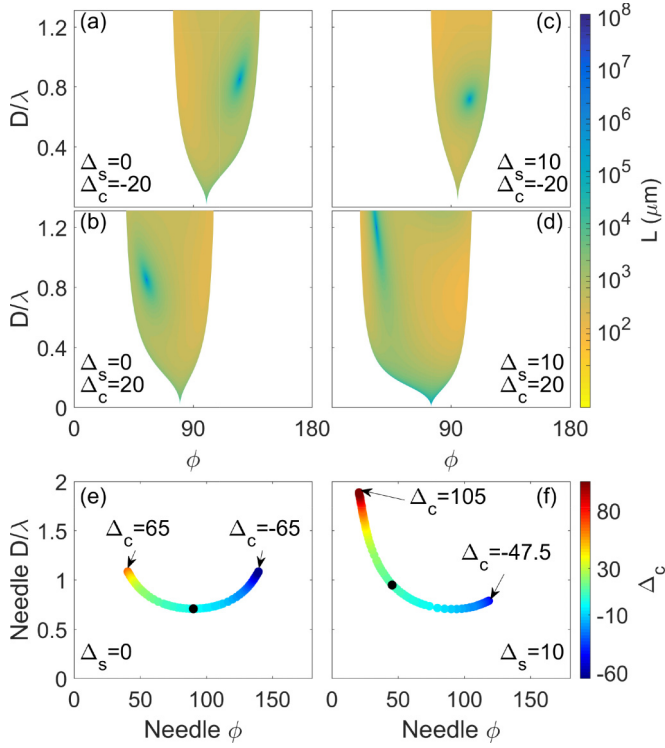


FIG. 4. Leaky-mode sheet for  $\Delta_s = 0^\circ$  and (a)  $\Delta_c = -20^\circ$  and (b)  $\Delta_c = +20^\circ$ . The leaky-mode sheet in (c) and (d) has the same values of  $\Delta_c$  but with  $\Delta_s = 10^\circ$ . Locus of the needle in the  $\phi - D/\lambda$  space under variation of  $\Delta_c$  for fixed values of (e)  $\Delta_s = 0^\circ$  and (f)  $\Delta_s = 10^\circ$ . The color of the dots in (e) and (f) indicates the value of  $\Delta_c$ . The black dot in each plot corresponds to the scenario  $\Delta_c = \Delta_s$  where the radiation channels are equivalent and instead of the needle the structure supports BIC lines of existence, as shown in Figs. 2(a) and 2(c).

exponential growth in the field profile as  $x \rightarrow \pm\infty$ . Figure 3(c), on the other hand, shows the profile of the same electric field component, but at the needle-BIC point. Since the BIC does not radiate, the field profile resembles a guided mode with exponential decay in the electric field outside the core.

The existence of the needle BIC is robust under variation of OA orientation, which only changes its position on the leaky-mode sheet, as illustrated in Fig. 4. The breaking of the symmetry around  $\phi = 90^\circ$  by setting  $\Delta_c, \Delta_s \neq 0^\circ$  determines the position of the needle, and the leaky-mode cutoff, as is shown by comparing Figs. 4(a)–4(d). In general, the greater the difference between  $\Delta_c$  and  $\Delta_s$ , the narrower the  $\phi$  range of existence of leaky modes, largely determining the range of  $\phi$  for which the needle exists. Figure 4(e) shows the locus of the needle in the  $\phi - D/\lambda$  space as a function of variation of  $\Delta_c$  with  $\Delta_s = 0^\circ$ . By setting a value of  $\Delta_s \neq 0^\circ$ , the symmetry of the locus is broken, allowing the tuning of the needle locus for a greater range of  $D/\lambda$  in terms of  $\Delta_c$  [Fig. 4(f)]. Varying the refractive index also changes the needle-BIC locus, similar to standard BICs in structures with full anisotropy-symmetry [31]. However, the needle is always present and only stops existing when it moves beyond the cutoff of the fundamental leaky mode on which it exists [extreme values of  $\Delta_c$  in Figs. 4(c) and 4(f)].

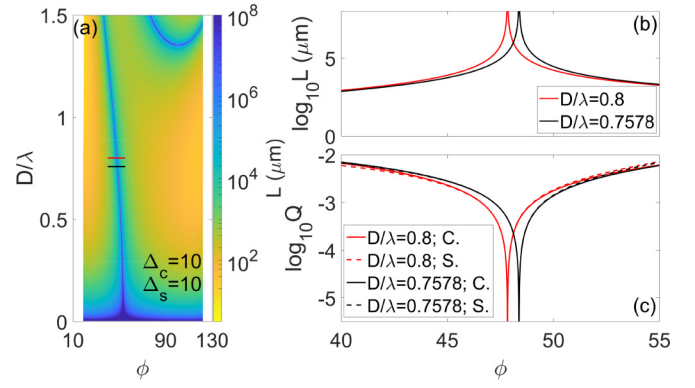


FIG. 5. (a) Same as Fig. 2(c) but showing red and black lines in the parameter space where we study the conditions for radiation suppression. (b) Logarithm of the propagation length  $L$  as a function of  $\phi$  at two different values of  $D/\lambda$ :  $D/\lambda = 0.8$  (red curve) and  $D/\lambda = 0.7578$  (black curve). The BICs occur at the point where  $L$  diverges. (c) Logarithm of  $Q$  corresponding to the cladding (C.),  $Q_c$  (solid curves), and the substrate (S.),  $Q_s$  (dashed curves), for the two values of  $D/\lambda$ .

## B. Conditions for radiation suppression

We study the solution of the conditions for radiation suppression in two different cases. Figure 5 shows the same scenario as Fig. 2(c) when the structure maintains mirror symmetry about  $x = D/2$ , though azimuthal anisotropy symmetry is broken equally in the cladding and the substrate ( $\Delta_c = \Delta_s = 10^\circ$ ). In this scenario, the two radiation channels are equivalent, and the fundamental leaky mode supports lines of INT BICs as shown in Fig. 5(a). We consider two different values of  $D/\lambda$ , 0.8 and 0.7578, and plot the propagation length  $L$  in terms of  $\phi$ . The results are shown in Fig. 5(b), which exhibits the typical signature of a diverging propagation length at the INT BIC position for both values of  $D/\lambda$ . In addition, Fig. 5(c) shows the logarithm for both  $Q_c$  and  $Q_s$  for the same range of  $\phi$ , and both  $Q_c$  and  $Q_s$  equal zero at the same value of  $\phi$  where  $L$  diverges, unequivocally indicating the presence of a BIC. As a result, we see that in a symmetric structure, a change in the value of  $D/\lambda$  results only in a shift in the value of  $\phi$  where BICs exist. Thus the system allows the suppression of radiation at different values of  $\phi$  via destructive interference in both the cladding and the substrate, resulting in the BIC. Consequently, the locus of the BIC in the  $\phi - D/\lambda$  space is the line (shown in dark blue) in Fig. 5(a).

Figure 6(a) shows the same scenario as Fig. 2(e), where the line of INT BICs collapses to a single needle BIC at  $D/\lambda = 0.7578$ . Here the mirror symmetry about the  $x = D/2$  plane is broken, while azimuthal anisotropy symmetry is broken in the cladding ( $\Delta_c = 10^\circ$ ) and maintained in the substrate ( $\Delta_s = 0^\circ$ ). Thus the radiation channels in the cladding and the substrate are now distinct. We see in Fig. 6(b) that the propagation length diverges at the INT BIC only when  $D/\lambda = 0.7578$ . As expected,  $Q_c$  and  $Q_s$  are zero at the value of  $\phi$  where the BIC exists for  $D/\lambda = 0.7578$  [Fig. 6(c)]. However, when we change the value of  $D/\lambda$  to 0.8, neither  $Q_c$  nor  $Q_s$  equals zero for any of the values of  $\phi$ . Thus, in this scenario, a shift in the value of  $D/\lambda$  from 0.7578 to 0.8 results in

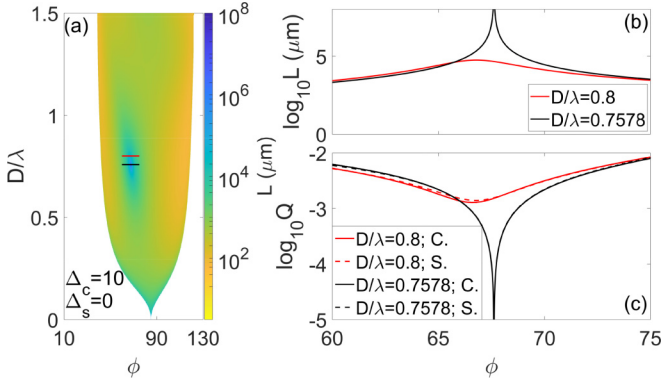


FIG. 6. (a)–(c) Same as Fig. 5 but for an asymmetric structure where azimuthal anisotropy symmetry is broken in the cladding ( $\Delta_c = 10^\circ$ ), but not in the substrate ( $\Delta_s = 0^\circ$ ).

the BIC disappearing. Therefore, in asymmetric structures with distinct radiation channels, the condition for radiation suppression for the cladding and substrate and the solution of the dispersion equation only have a simultaneous solution at a single point in the  $\phi - D/\lambda$  space where the needle BIC exists. Therefore the locus of the BIC in this structure is only a point on the leaky-mode sheet, resulting in the needle BIC.

We study this in more detail, examining the four auxiliary equations related to the condition for radiation suppression in the substrate. Figure 7(a) shows  $\text{Re}(N_{\text{aux}}^i)$  for  $D/\lambda = 0.7578$  (black curves in Fig. 6), corresponding to the existence of the needle BIC. In this scenario, the four solutions for the auxiliary equations  $N_{\text{aux}}^i$  and the solution of the dispersion equation [ $\text{Re}(N)$ ] coincide at a particular value of  $\phi$ . Therefore this is the point where  $Q_s$  equals zero in Fig. 6(c), meaning that it is possible to cancel the four tangential components of the radiation channel, resulting in the needle BIC. However, Fig. 7(b) illustrates the case of  $D/\lambda = 0.8$  (red curves in Fig. 6), showing that each solution  $N_{\text{aux}}^i$  intersects with  $\text{Re}(N)$  at different values of  $\phi$ . Each of the intersections is a point in  $\phi$  where the radiation channel is canceled when a set of three tangential field components is considered. However, there is no point where the solutions arising from all four sets of tangential field components intersect. Therefore BICs cannot exist at  $D/\lambda = 0.8$ . Though not shown here, the  $N_{\text{aux}}^i$  arising from the condition for radiation suppression in the cladding also shows similar behavior for the two cases shown in Fig. 7. This indicates that the cladding and substrate radiation channels are strongly coupled in this structure, and when the condition for radiation suppression is fulfilled in one channel, it is also fulfilled in the second one.

#### IV. DISCUSSION AND CONCLUSION

The transition in the dispersion diagram from BIC lines of existence to BIC points was introduced in Ref. [50]. In that work, the polar anisotropy symmetry was broken by taking the film OA out of the interface plane ( $\theta_f \neq 90^\circ$ ) in a structure with only one radiation channel. The result was multiple discrete INT BICs, avoiding the formation of an isolated needle

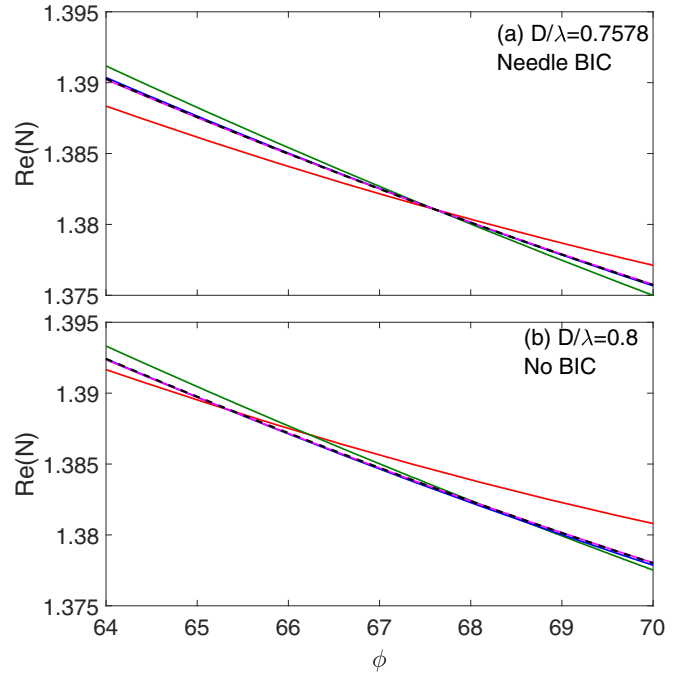


FIG. 7. Solution of the four auxiliary equations,  $N_{\text{aux}}^i$ , corresponding to the condition for radiation suppression in the substrate (solid colored curves) and the dispersion equation (dashed black line) for the structure in Fig. 6 with  $\Delta_c = 10^\circ$  and  $\Delta_s = 0^\circ$  for two different values of  $D/\lambda$ : (a)  $D/\lambda = 0.7578$  (existence of the needle BIC) and (b)  $D/\lambda = 0.8$  (no BIC). The condition for radiation suppression in the cladding yields similar results.

BIC. The existence of two distinct radiation channels leads to an additional constraint being placed on BIC existence and a consequent drop in dimension of the BIC solution from lines to points [5]. In this paper, the distinction between radiation channels is created by simultaneous breaking of azimuthal anisotropy symmetry and geometric mirror symmetry, leading to a single spectrally isolated BIC that for practical purposes is the only bound state supported by the otherwise antiguiding structures.

Needle BICs occur as robust phenomena, and their loci on the leaky-mode sheet can be tuned under variation of the OA orientation. Nevertheless, the latter property is more complex than the interpretation of finding the point of intersection of two independent solutions corresponding to cladding and substrate radiation channels. The results shown here should be seen in light of the interference between the two radiation channels through the reflections in the film layer, which are included in the transfer matrix  $\hat{M}$ , and the condition for radiation suppression, carried by Eqs. (9) and (10). In particular, the analysis of the conditions for radiation suppression for each radiation channel shows that the reason for the collapse of INT BIC lines in symmetric structures to needle BICs in asymmetric structures is the impossibility of simultaneously canceling all four tangential components of the radiation channel.

Needle BICs have been shown here in the simplest geometry, but we have verified that they also occur in other configurations, e.g., with broken polar anisotropy symmetry.

We thus anticipate that analogous phenomena may occur in other open systems with two differentiated radiation channels featuring an isolated needle BIC offering the possibility of simultaneous spatial and spectral filtering. This is an interesting feature that can inspire new schemes in the case of the applications of BICs in lasing [36,37], ultrastable lasers [63], and the scaling up of cavity dimensions preserving single-mode operation [64], while the needle-BIC parametric tuning suggests applications in optical communications [39].

## ACKNOWLEDGMENTS

This work was supported by H2020 Marie Skłodowska-Curie Action GA665884; Agencia Estatal de Investigación Grants No. CEX2019-000910-S 315, No. PGC2018-097035-B-I00, and No.PID2022-138280NB-I00 funded by MCIN/AEI/316 10.13039/501100011033/FEDER; and CERCA, Departament de Recerca i Universitats de la Generalitat de Catalunya (2021 SGR 01448), Fundació Cellex, and Fundació Mir-Puig.

- 
- [1] J. von Neumann and E. Wigner, Über merkwürdige diskrete Eigenwerte: Über das Verhalten von Eigenwerten bei adiabatischen Prozessen, *Z. Phys.* **30**, 467 (1929).
- [2] F. H. Stillinger and D. R. Herrick, Bound states in the continuum, *Phys. Rev. A* **11**, 446 (1975).
- [3] H. Friedrich and D. Wintgen, Interfering resonances and bound states in the continuum, *Phys. Rev. A* **32**, 3231 (1985).
- [4] R. Parker, Resonance effects in wake shedding from parallel plates: Some experimental observations, *J. Sound Vib.* **4**, 62 (1966).
- [5] C. W. Hsu, B. Zhen, A. D. Stone, J. D. Joannopoulos, and M. Soljačić, Bound states in the continuum, *Nat. Rev. Mat.* **1**, 16048 (2016).
- [6] K. Koshelev, G. Favraud, A. Bogdanov, Y. Kivshar, and A. Fratalocchi, Nonradiating photonics with resonant dielectric nanostructures, *Nanophotonics* **8**, 725 (2019).
- [7] S. Joseph, S. Pandey, S. Sarkar, and J. Joseph, Bound states in the continuum in resonant nanostructures: An overview of engineered materials for tailored applications, *Nanophotonics* **10**, 4175 (2021).
- [8] A. F. Sadreev, Interference traps waves in an open system: Bound states in the continuum, *Rep. Prog. Phys.* **84**, 055901 (2021).
- [9] D. C. Marinica, A. G. Borisov, and S. V. Shabanov, Bound states in the continuum in photonics, *Phys. Rev. Lett.* **100**, 183902 (2008).
- [10] E. N. Bulgakov and A. F. Sadreev, Bound states in the continuum in photonic waveguides inspired by defects, *Phys. Rev. B* **78**, 075105 (2008).
- [11] Y. Plotnik, O. Peleg, F. Dreisow, M. Heinrich, S. Nolte, A. Szameit, and M. Segev, Experimental observation of optical bound states in the continuum, *Phys. Rev. Lett.* **107**, 183901 (2011).
- [12] G. Corrielli, G. Della Valle, A. Crespi, R. Osellame, and S. Longhi, Observation of surface states with algebraic localization, *Phys. Rev. Lett.* **111**, 220403 (2013).
- [13] C. W. Hsu, B. Zhen, J. Lee, S.-L. Chua, S. G. Johnson, J. D. Joannopoulos, and M. Soljačić, Observation of trapped light within the radiation continuum, *Nature (London)* **499**, 188 (2013).
- [14] S. I. Azzam, V. M. Shalaev, A. Boltasseva, and A. V. Kildishev, Formation of bound states in the continuum in hybrid plasmonic-photonic systems, *Phys. Rev. Lett.* **121**, 253901 (2018).
- [15] S. Joseph, S. Sarkar, S. Khan, and J. Joseph, Exploring the optical bound state in the continuum in a dielectric grating coupled plasmonic hybrid system, *Adv. Opt. Mater.* **9**, 2001895 (2021).
- [16] L. S. Li, J. Zhang, C. Wang, N. Zheng, and H. Yin, Optical bound states in the continuum in a single slab with zero refractive index, *Phys. Rev. A* **96**, 013801 (2017).
- [17] M. Minkov, I. A. D. Williamson, M. Xiao, and S. Fan, Zero-index bound states in the continuum, *Phys. Rev. Lett.* **121**, 263901 (2018).
- [18] F. Monticone and A. Alù, Bound states within the radiation continuum in diffraction gratings and the role of leaky modes, *New J. Phys.* **19**, 093011 (2017).
- [19] L. L. Doskolovich, E. A. Bezus, and D. A. Bykov, Two-groove narrowband transmission filter integrated into a slab waveguide, *Photonics Res.* **6**, 61 (2018).
- [20] D. A. Bykov, E. A. Bezus, and L. L. Doskolovich, Bound states in the continuum and strong phase resonances in integrated Gires-Tournois interferometer, *Nanophotonics* **9**, 83 (2020).
- [21] K. Fan, I. V. Shadrivov, and W. J. Padilla, Dynamic bound states in the continuum, *Optica* **6**, 169 (2019).
- [22] S. Han, L. Cong, Y. K. Srivastava, B. Qiang, M. V. Rybin, A. Kumar, R. Jain, W. X. Lim, V. G. Achanta, S. S. Prabhu, Q. J. Wang, Y. S. Kivshar, and R. Singh, All-dielectric active terahertz photonics driven by bound states in the continuum, *Adv. Mater.* **31**, 1901921 (2019).
- [23] Y. Liang, K. Koshelev, F. Zhang, H. Lin, S. Lin, J. Wu, B. Jia, and Y. Kivshar, Bound states in the continuum in anisotropic plasmonic metasurfaces, *Nano Lett.* **20**, 6351 (2020).
- [24] Y. Chen, H. Deng, X. Sha, W. Chen, R. Wang, Y.-H. Chen, D. Wu, J. Chu, Y. S. Kivshar, S. Xiao, and C.-W. Qiu, Observation of intrinsic chiral bound states in the continuum, *Nature (London)* **613**, 474 (2023).
- [25] E. N. Bulgakov and A. F. Sadreev, Robust bound state in the continuum in a nonlinear microcavity embedded in a photonic crystal waveguide, *Opt. Lett.* **39**, 5212 (2014).
- [26] E. N. Bulgakov and A. F. Sadreev, Light trapping above the light cone in a one-dimensional array of dielectric spheres, *Phys. Rev. A* **92**, 023816 (2015).
- [27] E. N. Bulgakov and A. F. Sadreev, Bound states in the continuum with high orbital angular momentum in a dielectric rod with periodically modulated permittivity, *Phys. Rev. A* **96**, 013841 (2017).
- [28] A. Cerjan, C. W. Hsu, and M. C. Rechtsman, Bound states in the continuum through environmental design, *Phys. Rev. Lett.* **123**, 023902 (2019).
- [29] A. I. Ovcharenko, C. Blanchard, J.-P. Hugonin, and C. Sauvan, Bound states in the continuum in symmetric and asymmetric photonic crystal slabs, *Phys. Rev. B* **101**, 155303 (2020).
- [30] J. Gomis-Bresco, D. Artigas, and L. Torner, Anisotropy-induced photonic bound states in the continuum, *Nat. Photonics* **11**, 232 (2017).



- [31] S. Mukherjee, J. Gomis-Bresco, P. Pujol-Closa, D. Artigas, and L. Torner, Angular control of anisotropy-induced bound states in the continuum, *Opt. Lett.* **44**, 5362 (2019).
- [32] I. V. Timofeev, D. N. Maksimov, and A. F. Sadreev, Optical defect mode with tunable  $Q$  factor in a one-dimensional anisotropic photonic crystal, *Phys. Rev. B* **97**, 024306 (2018).
- [33] P. S. Pankin, B.-R. Wu, J.-H. Yang, K.-P. Chen, I. V. Timofeev, and A. F. Sadreev, One-dimensional photonic bound states in the continuum, *Commun. Phys.* **3**, 91 (2020).
- [34] Z. Liu, X. Li, C. Chen, X. Wang, W. Gao, W. Ye, L. Li, and J. Liu, Bound states in the continuum in asymmetric one-dimensional photonic crystal systems guided by anisotropy, *Opt. Express* **31**, 8384 (2023).
- [35] S. Mukherjee, D. Artigas, and L. Torner, Surface bound states in the continuum in Dyakonov structures, *Phys. Rev. B* **105**, L201406 (2022).
- [36] A. Kodigala, T. Lepetit, Q. Gu, B. Bahari, Y. Fainman, and B. Kanté, Lasing action from photonic bound states in continuum, *Nature (London)* **541**, 196 (2017).
- [37] B. Midya and V. V. Konotop, Coherent-perfect-absorber and laser for bound states in a continuum, *Opt. Lett.* **43**, 607 (2018).
- [38] S. Romano, A. Lamberti, M. Masullo, E. Penzo, S. Cabrini, I. Rendina, and V. Mocella, Optical biosensors based on photonic crystals supporting bound states in the continuum, *Materials* **11**, 526 (2018).
- [39] Z. Yu, Y. Tong, H. K. Tsang, and X. Sun, High-dimensional communication on etchless lithium niobate platform with photonic bound states in the continuum, *Nat. Commun.* **11**, 2602 (2020).
- [40] N. Rivera, C. W. Hsu, B. Zhen, H. Buljan, J. D. Joannopoulos, and M. Soljačić, Controlling directionality and dimensionality of radiation by perturbing separable bound states in the continuum, *Sci. Rep.* **6**, 33394 (2016).
- [41] X. Yin, J. Jin, M. Soljačić, C. Peng, and B. Zhen, Observation of topologically enabled unidirectional guided resonances, *Nature (London)* **580**, 467 (2020).
- [42] Z. Hayran and F. Monticone, Capturing broadband light in a compact bound state in the continuum, *ACS Photonics* **8**, 813 (2021).
- [43] M. V. Rybin, K. L. Koshelev, Z. F. Sadrieva, K. B. Samusev, A. A. Bogdanov, M. F. Limonov, and Y. S. Kivshar, High- $Q$  supercavity modes in subwavelength dielectric resonators, *Phys. Rev. Lett.* **119**, 243901 (2017).
- [44] J. Jin, X. Yin, L. Ni, M. Soljačić, B. Zhen, and C. Peng, Topologically enabled ultrahigh- $Q$  guided resonances robust to out-of-plane scattering, *Nature (London)* **574**, 501 (2019).
- [45] L. Carletti, K. Koshelev, C. De Angelis, and Y. Kivshar, Giant nonlinear response at the nanoscale driven by bound states in the continuum, *Phys. Rev. Lett.* **121**, 033903 (2018).
- [46] Z. Liu, Y. Xu, Y. Lin, J. Xiang, T. Feng, Q. Cao, J. Li, S. Lan, and J. Liu, High- $Q$  quasibound states in the continuum for nonlinear metasurfaces, *Phys. Rev. Lett.* **123**, 253901 (2019).
- [47] O. Gbidi and C. Shen, Selectively exciting quasibound states in the continuum in open microwave resonators using dielectric scatters, *Phys. Rev. B* **107**, 184309 (2023).
- [48] Y. Chen, M. Li, J. Wang, and M. Zhao, Polarization-selective excitation of multiband quasibound states in the continuum supported by symmetry-perturbed silicon metasurface, *Opt. Commun.* **527**, 128904 (2023).
- [49] S. Mukherjee, J. Gomis-Bresco, D. Artigas, and L. Torner, Unidirectional guided resonances in anisotropic waveguides, *Opt. Lett.* **46**, 2545 (2021).
- [50] S. Mukherjee, J. Gomis-Bresco, P. Pujol-Closa, D. Artigas, and L. Torner, Topological properties of bound states in the continuum in geometries with broken anisotropy symmetry, *Phys. Rev. A* **98**, 063826 (2018).
- [51] M. W. McCall, I. J. Hodgkinson, and Q. Wu, *Birefringent Thin Films and Polarizing Elements*, 2nd ed. (Imperial College Press, London, 2015).
- [52] D. W. Berreman, Optics in stratified and anisotropic media: 4  $\times$  4-matrix formulation, *J. Opt. Soc. Am.* **62**, 502 (1972).
- [53] D. Marcuse and I. Kaminow, Modes of a symmetric slab optical waveguide in birefringent media - Part II: Slab with coplanar optical axis, *IEEE J. Quantum Electron.* **15**, 92 (1979).
- [54] A. Knoesen, T. K. Gaylord, and M. G. Moharam, Hybrid guided modes in uniaxial dielectric planar waveguides, *J. Lightwave Technol.* **6**, 1083 (1988).
- [55] L. Torner, J. Rekolons, and J. P. Torres, Guided-to-leaky mode transition in uniaxial optical slab waveguides, *J. Lightwave Technol.* **11**, 1592 (1993).
- [56] J. Hu and C. R. Menyuk, Understanding leaky modes: Slab waveguide revisited, *Adv. Opt. Photonics* **1**, 58 (2009).
- [57] O. Takayama, L.-C. Crasovan, S. K. Johansen, D. Mihalache, D. Artigas, and L. Torner, Dyakonov surface waves: A review, *Electromagnetics* **28**, 126 (2008).
- [58] K. Koshelev, S. Lepeshov, M. Liu, A. Bogdanov, and Y. Kivshar, Asymmetric metasurfaces with high- $Q$  resonances governed by bound states in the continuum, *Phys. Rev. Lett.* **121**, 193903 (2018).
- [59] Z. F. Sadrieva, I. S. Sinev, K. L. Koshelev, A. Samusev, I. V. Iorsh, O. Takayama, R. Malureanu, A. A. Bogdanov, and A. V. Lavrinenko, Transition from optical bound states in the continuum to leaky resonances: Role of substrate and roughness, *ACS Photonics* **4**, 723 (2017).
- [60] B. Zhen, C. W. Hsu, L. Lu, A. D. Stone, and M. Soljačić, Topological nature of optical bound states in the continuum, *Phys. Rev. Lett.* **113**, 257401 (2014).
- [61] E. N. Bulgakov and D. N. Maksimov, Topological bound states in the continuum in arrays of dielectric spheres, *Phys. Rev. Lett.* **118**, 267401 (2017).
- [62] H. M. Doeleman, F. Monticone, W. den Hollander, A. Alù, and A. F. Koenderink, Experimental observation of a polarization vortex at an optical bound state in the continuum, *Nat. Photonics* **12**, 397 (2018).
- [63] D. G. Matei, T. Legero, S. Häfner, C. Grebing, R. Weyrich, W. Zhang, L. Sonderhouse, J. M. Robinson, J. Ye, F. Riehle, and U. Sterr, 1.5  $\mu\text{m}$  lasers with sub-10 mHz linewidth, *Phys. Rev. Lett.* **118**, 263202 (2017).
- [64] R. Contractor, W. Noh, W. Redjem, W. Qarony, E. Martin, S. Dhuey, A. Schwartzberg, and B. Kanté, Scalable single-mode surface-emitting laser via open-Dirac singularities, *Nature (London)* **608**, 692 (2022).